The Theory of Velocity Selective Neural Recording: A Study Based on Simulation

John Taylor[1], Martin Schuettler[2], Chris Clarke[1] and Nick Donaldson[3]

1. Department of Electronic and Electrical Engineering, University of Bath, Bath UK
2. Laboratory for Biomedical Microtechnology, Department of Microsystems Engineering – IMTEK, University of Freiburg, 79110 Freiburg, Germany.
3. Department Medical Physics and Bioengineering, University College London, London WC1 UK.

Corresponding author: John Taylor. Tel +44 (0)1225 38 3910; email j.t.taylor@bath.ac.uk

Abstract- This paper describes improvements to the theory of *velocity selective recording* and some simulation results. In this method, activity is different groups of axons is discriminated by their propagation velocity. A multi-electrode cuff and an array of amplifiers produce multiple neural signals; if artificial delays are inserted and the signals are added, the activity in axons of the matched velocity are emphasized. We call this *intrinsic velocity selective recording*. However, simulation shows that interpreting the time signals is then not straight-forward and the selectivity Q_v is low. New theory shows that bandpass filters improve the selectivity and explains why this is true in the time domain. A simulation study investigates the limits on the available velocity selectivity both with and without additive noise and with reasonable sampling rates and analogue-to-digital conversion (ADC) parameters. Bandpass filters can improve the selectivity by factors up to 7 but this depends on the speed of the action potential and the signal-to-noise ratio.

Keywords: Electroneurogram recording, Simulation, Multielectrode cuffs, Velocity selective recording

Total text words: 5848
Words in the abstract: 159
Number of figures: 6
Number of Tables: 2

1. Introduction

Velocity selective recording (VSR) is a technique which should allow more information to be extracted from an intact nerve with a recording set-up that does not allow action potentials from single fibres to be seen at spikes [9, 1]. The method is in essence very simple and relies on taking measurements of a propagating *action potential* (AP) at two or more points. The distance between the sample points divided by the delay between two appearance of the AP provides a measure of the propagation velocity. Conversely, artificially delaying one or more signals before adding them gives a maximum response at the matched velocity. This simple idea is not new and various researchers have investigated practical adaptations of it in the past-*e.g.* [6, 11, 2, 3].

However, at present the idea has not been demonstrated with naturally-occurring nerve traffic though experimenters have used *multi-electrode cuffs* (MECs) to observe appropriate outputs from compound action potentials [5, 6, 11]. Two papers about the theory of VSR have been published by the same authors [9, 1]. The first presented a spectral analysis of a single axon in an MEC with a *tripolar* (double-differential) amplifier system and the signal processing arrangement shown in Figure 1. The bandpass filter (BPF) that follows the adder was shown to improve selectivity in the *velocity domain*, however the filters were ideal and of infinitesimal bandwidth. We envisage that a useful VSR system might actually have several signal processing units (Figure 1), each matched to one of the propagation velocities of functional significance [9].

The second theory paper [1] considered the thermal noise generated by the detection system and compared its amplitude to that of the signal resulting from the summation of multiple *single fibre action potentials* (SFAPs) which were assumed to occur at random times. This allowed the firing rates required from various sizes of nerve fibre in a given MEC to provide a signal that could be detected above the background noise to be calculated.

The current paper presents material which supplements and expands our earlier work [9, 1]. In essence it is a study (by simulation) of improvements in velocity selectivity obtainable by the use of BPFs, investigating in particular the limitations of the method with and without noise. The intended outcome of this work is to achieve a significant improvement in the performance of VSR systems so that they can be employed to discriminate between populations of naturally-occurring APs. As already noted, the relatively poor velocity selectivity of the VSR systems tested to date has limited their application to CAPs.

Deterministic models of nerve signals (i.e. SFAPs) are used exclusively in the study, the effects of random signal generation being reserved for presentation in a subsequent paper.

2. Methods

2.1 Basic principles

The response of an MEC to a propagating SFAP has been discussed in detail elsewhere and is only very briefly summarised here [9, 1]. The input to the MEC is a *trans-membrane action potential* function (TMAP), $V_m(t)$, with the corresponding spectrum $V_m(f)$. The resulting SFAP is a propagating wave with the time dependence of the underlying TMAP function, the relationship between the two being explained in [9]. For the purpose of simulation, we represent the TMAP function and its spectrum by the Fourier transform pair [1]:

$$V_m(t) = At^n e^{-Bt}$$

$$V_m(f) = \frac{n!A}{(B + j2\pi f)^{n+1}} \qquad \ldots (1)$$

where A, B and n are constants and f is frequency (the symbology has been preserved from [9]). This function has been proposed as a suitable basis for the simulation of mammalian ENG [8, 7, 10]. The output $Y(f, v)$, which is a function of both frequency and velocity, is obtained by treating the MEC as a linear time-invariant system with transfer function $H(f, v)$:

$$Y(f,v) = G(f,v)\cdot H_0(f,v)\cdot V_m(f) = \left|\frac{\sin\left(N\pi f\left(\frac{d}{v}-\tau\right)\right)}{\sin\left(\pi f\left(\frac{d}{v}-\tau\right)\right)}\right| \cdot 4\frac{R_e}{R_a}\sin^2\left(\frac{\pi f d}{v}\right)\cdot\left|\frac{An!}{(B+j2\pi f)^{n+1}}\right| \quad \ldots. (2)$$

This equation describes the output of a cuff with N tripoles, electrode pitch d and propagation velocity v. R_a, the intra-axonal resistance per unit length, has been assumed to be large compared to R_e, the extra-axonal resistances per unit length inside the cuff. The artificial time delays are multiples of τ (see [1] for a full explanation). Equation 2 is the product of the spectrum of the TMAP ($V_m(f)$), the transfer function

of one tripole ($H_o(f,v)$), and the transfer function of the delay-and-add block ($G(f,v)$). At *matched velocities* (i.e. where $\tau = d/v$ and $v = v_o$ in eqn (2)), eqn (2) reduces to:

$$Y(f, v_0) = 4N \frac{R_e}{R_a} \sin^2\left(\frac{\pi f d}{v_0}\right) \cdot \left| \frac{An!}{(B + j2\pi f)^{n+1}} \right| \qquad \ldots (3)$$

The output of the system $Y(f,v)$ is a function of two variables and it was pointed out in [9] that if f is fixed by passing the output through a bandpass filter (so that $f = f_0$), Y becomes a function of propagation velocity v only, enabling the *velocity selectivity* profile (see the *tuning curves* in [9]) to be calculated.

We define a *velocity quality factor*, Q_v, by analogy with linear systems in the frequency domain [1]:

$$Q_v = \frac{v_0}{v_{3+} - v_{3-}} \qquad \ldots (4)$$

where v_0 is the matched (i.e. peak) velocity and v_{3+} and v_{3-} are the velocities at which the output has fallen to $1/\sqrt{2}$ (-3 dB) of the peak value. Close to the matched velocities, the velocity selectivity is dominated by the function $G(f,v)$ and an approximate formula for Q_v was derived in [1]:

$$Q_v \cong \frac{N\pi f_0 d}{2.64 v_0} \qquad \ldots (5)$$

Q_v and its approximation (eqn (5)) will be used to characterise velocity profiles in this paper.

2.2 The intrinsic velocity spectrum (IVS)

If bandpass filtering is not applied, as noted above, the output will depend on v and on frequency dependent elements in the system including the spectral properties of the input signal (i.e. the TMAP function) and the characteristics of the channel. For these reasons, unlike the bandpass filtered version, the resulting time domain function is difficult to interpret. Simulating in the time domain, Fig 2 is the time-domain output of the adder in Fig 1 when the system is stimulated with a TMAP resulting in an SFAP propagating at a velocity of 30 m/s. Two TMAP functions are considered, based on equation (1), with the parameters given in Figs 2(b) and 2(c) (the scaling parameter A has been adjusted in both cases so that the peak amplitudes of the functions are normalised to unity). The matched velocity v_o is treated as a parameter leading to the family of curves shown in Fig 2(a). The peak value is reached when the

artificial delays exactly match (cancel) the naturally-occurring delays at which point the output signal has the same form as a single SFAP, with amplitude multiplied by N [1].

Fig 2(b) shows the IVS of the system, stimulated by an SFAP generated by TMAP#1 (and repeated in Fig 2(c) for TMAP#2). This is a plot of the peak values of the output time record (Fig 2(a)) as a function of propagation velocity after the tripole signals have been subjected to delay and add operations *only*. Each curve in the time record shown in Fig 2(a) has three peaks, labelled α, β and γ, two positive and one negative, corresponding to the phases of the tripolar SFAP. Whilst it is possible to calculate the IVS using the height of any of these peaks as the amplitude, this paper considers only the two larger-amplitude peaks, α and β. The resulting spectra peak at the same matched velocity (40 m/s), but have different selectivities as shown in Fig 2(b), where the two IVS plots are shown together with the values of Q_v calculated from the figure using eqn (4). These values of intrinsic velocity selectivity are used as baseline references for the enhancements described in the next section.

From the above observations, it is clear that if this method is to be used to separate neural signals in terms of velocity, certain problems of interpretation arise:

1. The measured IVS depends on the point in the time response of the delayed and summed signal used to make the measurement;
2. The IVS profile depends on the properties of the TMAP function, in particular, shorter responses result in larger values of Q_v;
3. The actual selectivity obtainable is quite low and declines with increasing velocity. This accords with the theory presented below (see also [1]).

These issues are considered in the next section.

2.3 Improved Velocity Selective Recording Using Bandpass Filters (BPFVS)

The theory presented in our earlier papers and summarized above described the operation of a delay-matched VSR system in the *velocity* domain. However in order to understand better the generation of the IVS using this method and especially the enhancements possible using bandpass filters (BPFVS), a time domain interpretation is very useful. Consider the representation of the tripolar amplifier outputs in Fig 1 by N, equally-spaced rectangular pulses of arbitrary height h and duration δt. The delay between adjacent tripolar outputs is τ and that this is related to the SFAP propagation velocity v and the inter-electrode spacing d as follows:

$$\tau = \frac{d}{v} \qquad \ldots (6)$$

Clearly if the N pulses are summed and $\delta t < \tau$, the result will be a train of pulses of height h and spacing $\tau - \delta t$. If , on the other hand, artificial delays are introduced to cancel the naturally-occurring delays as shown in the signal processing unit in Fig 1, the summed output will be a single pulse of duration δt and height $N.h$. Between these extreme cases lie intermediate states where the externally applied delay is not exactly equal to τ and hence the delay is not exactly matched. The rapidity of the transition through these intermediate states determines the velocity selectivity and Q_v. As the inserted delay is increased from zero, the pulses begin to overlap and it is easy to see that the value of inserted delay required for this to happen depends on both τ *and on* δt, *the width of the pulses themselves*. So, in order to produce a summed output of particular amplitude, the value of the inserted delay is required to be closer to τ than would be the case for wider pulses (adding more pulses-increasing N-has a similar effect). *This is observed as an increase in intrinsic velocity selectivity for narrower pulses*. In summary, we can draw the following initial conclusions regarding intrinsic *delay matched* VSR:

1. The *intrinsic velocity selectivity*, Q_v is inversely proportional to the width of the tripolar SFAP pulses and therefore strongly dependent on the spectral content of the underlying TMAP function;
2. Q_v is proportional to N, the order of the system (number of tripoles).

The proposed approach to reducing the sensitivity to the TMAP is to place a BPF at the output of each tripolar amplifier of the VSR system. The impulse response of a bandpass filter is a burst of damped sinewaves whose frequency is the centre frequency of the BPF while the duration of the burst depends on the filter order and relative bandwidth. For example, Fig 3(a) shows the response of an 8^{th} order Butterworth BPF of centre frequency 1 kHz and relative bandwidth 20% to a narrow pulse of unit amplitude. Since the same type of response is elicited by stimulating a BPF with a tripolar action potential, the 'delay matching' process is transformed into matching delayed *sinewaves* rather than complex SFAP waveforms as in the intrinsic case. Unlike the SFAP waveform itself, the BPF output has no dependence on the characteristics of the TMAP except for its amplitude and its exact position in the time record. The addition of BPFs in this way therefore allows the measurement of velocity selectivity to be decoupled from the spectral properties of the TMAP and to be controlled by means of the centre frequency of the filters which is to some extent a free parameter. Note that although the proposed arrangement requires a BPF at the output of each tripolar channel, in practice, due to the linearity of the processes involved, the summation and filtering operations can be reversed. This leads to the much simpler and more practical arrangement of Fig 1, where only a single BPF is required.

In order to determine the velocity spectrum obtained by delay matching with BPFs, it is sufficient to calculate the peak value of the output as a function of inserted delay. As already noted, the transient response of a BPF is a burst of damped sinewaves (see Fig 3(a)) and so the overall response of the system, *f(t)*, close to the point of exact match can be represented as the sum of *N* sinewaves, a simplified example of which is shown in Fig 3(b). Each of the three sinewaves shown in the figure represents the sinewave at the centre of the burst at the output of each BPF. For simplicity, the origin of the time axis has been placed at the centre of the set of sinewaves (so that when the signals are matched they peak at *t* = 0) and the amplitudes of the sinewaves have been normalised to unity. The period of the sinewaves is *T*, which is the inverse of f_0, where f_0 is the centre frequency of the BPF and the offset due to the passage of the AP along the MEC is τ. The result of adding the *N* sinewaves where *N* is odd (similar principles apply for *N* even) is:

$$f(t) = \cos\omega_0\left(t + \frac{N-1}{2}\tau\right) + \ldots + \cos\omega_0 t + \ldots + \cos\omega_0\left(t - \frac{N-1}{2}\tau\right) \qquad \ldots (7)$$

where $\tau = d/v_0$ and $\omega_0 = 2\pi f_0$. This function reaches a maximum at $t = 0$ for any values of *N* and τ and so, to consider the selectivity, eqn (7) is rewritten:

$$f(t)\big|_{t=0} = \cos\omega_0\left(\frac{N-1}{2}\tau\right) + \ldots + 1 + \ldots + \cos\omega_0\left(\frac{N-1}{2}\tau\right) \qquad \ldots (8)$$

So, for example, for $N = 3$:

$$f_3(t)\big|_{t=0} = 1 + 2\cos\omega_0\tau$$

for $N = 5$:

$$f_5(t)\big|_{t=0} = 1 + 2\cos\omega_0\tau + 2\cos 2\omega_0\tau$$

and so on.

After some manipulation, it is possible to show for the general case that:

$$f_N(t)\big|_{t=0} = \left(2\cos\frac{\omega_0\tau}{2}\right)^{N-1} - {}^{N-2}C_1\left(2\cos\frac{\omega_0\tau}{2}\right)^{N-3} + {}^{N-3}C_2\left(2\cos\frac{\omega_0\tau}{2}\right)^{N-5} - \ldots$$

where the series terminates when the exponent is zero. The sum of this standard finite series is given in eqn (9).

$$= \frac{\sin N(\omega_0 \tau / 2)}{\sin(\omega_0 \tau / 2)} \qquad \ldots (9)$$

Eqn (9) is just the function *G* from eqn (2) except that, as already noted, the delay (τ) shown in eqn (2) has been normalised so that it actually represents offsets from the matched value. This is the formula derived in [1] by spectral (velocity domain) analysis, showing that the two views of the method are consistent.

2.4 The influence of analogue bandwidth and analogue-to-digital conversion

Figure 4 shows the frequency spectrum of a 9-tripole IVS system with an inter-electrode spacing (*d*) of 3 mm, SFAP derived from both the TMAPs considered in this paper and matched at a propagation velocity of 30 m/s. The sample rate is 100 ks/s and the resolution of the analogue to digital converter (ADC) is 10 bits, both requirements being realisable in a practical system. In the matched case (i.e. $v = v_0$), as already noted, the transfer function of the system is just that for a single tripole multiplied by *N* (see eqns (2) and (3)):

$$H_m(v_0, f) = 4N \frac{R_e}{R_a} \sin^2(\pi f d / v_0) \propto v^2 \sin^2(\pi f d / v_0)$$

The transmission zeros of this function occur at the following frequencies:

$$f = \frac{v_0}{d} m; \quad m = 0, 1, 2, 3, \ldots \qquad \ldots (10)$$

where the sequence extends in theory to the Nyquist limit ($f_s/2$, where f_s is the sampling frequency) but in practice is likely to be limited by the finite bandwidth of the analogue channels, the constraints of ADC and noise. Examination of these spectra indicates that the amplitude of TMAP #2 declines much more slowly with frequency than that of TMAP #1. As a result, due to the wider bandwidth of the TMAP #2 spectrum, the dynamic range is reduced compared to TMAP #1, easing the demands on ADC. Operation at higher frequencies, approaching the Nyquist limit is therefore possible for TMAP #2 if the analogue channel bandwidth permits it. This in turn permits much higher levels of selectivity, since this is proportional to frequency (see eqn (5)). In summary, for the two TMAPs considered, the limiting factor for TMAP #1 is ADC resolution, whereas in the case of TMAP #2 it is determined by analogue bandwidth and the Nyquist limit. It should be noted, of course that any selectivity enhancements are subject to the degrading effects of noise. This aspect is dealt with in Section 3 below.

2.5 The significance of bandpass filter order

Fig 5 demonstrates the effect and importance of *filter order* on the behaviour of a VSR system. As described above, the bandpass filter added at the output of an IVSR system is required to produce a burst of damped sinusoidal oscillation at the centre frequency of the BPF when stimulated with a wide band signal such as an SFAP. For this to happen, the filter must reject out-of-band signals that would otherwise corrupt its response. In particular, the 'baseband' (borrowing some terminology from communication systems) SFAP signal generated from TMAP#1 peaks at about 1.5 kHz and has a much larger amplitude than the 'harmonics' further up the frequency scale. The figure shows that this is still true for a $p = 2$ Butterworth bandpass filter since the filtered spectral amplitude at frequencies in the range 0-5 kHz is actually larger than in the passband. This suggests the need for a BPF with $p = 4$, at least. The small insets in the corners of the figure show the effect of filter order in the time domain. For $p = 2$, for example, the filter output is dominated by the SFAP input signal, which is consistent with the frequency domain situation. By contrast, for $p = 8$ the input signal has been suppressed and the output is a symmetrical burst of damped sinusoids. Note however that p cannot be increased without limit because, as the filter order is increased, the time domain response becomes longer. As discussed in Section 2.6, this tends to increase the prevalence of false 'image' outputs. In addition, the requirement for higher filter order tends to increase the ratios of the digital filter coefficients, making realisation more difficult.

2.6 Generation of spurious responses

One of the effects of using BPFs to enhance the performance of IVSR is the potential for the generation of spurious velocity spectral responses ('images'). These occur because single tripolar SFAP waveforms are replaced by bursts of damped sinewaves of frequency f_o, the centre frequency of a BPF. Therefore, although a global maximum occurs when all the signals are matched, with or without BPFs, the potential exists for subsidiary, 'image' responses to be generated when the signals are mismatched by integer multiples of the period of the sinewaves, $1/f_o$. Images will be generated if and only if:

$$W \geq N \qquad \ldots (11)$$

where W is the number of cycles of sinewave in each burst and N is order of the system (i.e., the number of tripolar channels being delay-matched) and that the velocity at which the images are formed is given by:

$$v_{image} = \frac{d}{\tau \pm q / f_o} \qquad \ldots (12)$$

where d is the inter-electrode spacing, τ is the naturally-occurring delay and q is an integer. Note that the velocities at which image responses occur depend on f_o, the centre frequency of the BPF, in contrast to an output resulting from an excited population which will appear at the same velocity irrespective of f_o. In addition, for practical values of the other parameters in eqn (10), the images tend to occur at velocities that lie outside the band of interest (say 20 – 120 m/s). For these reasons, images are easily distinguished from genuine outputs, as illustrated in Fig 6.

3. Results

3.1 Simulated results without noise

In order to demonstrate the effects of adding BPFs to a delay-matched IVS system, the MATLAB simulations shown in Fig 2 were repeated with a single bandpass filter of centre frequency f_0 placed at the output of the system, as shown in Fig 1. The SFAPs were generated using TMAP#1 and TMAP#2 and the system was noiseless. The filter was an 8^{th}-order digital Butterworth BPF and centre frequencies of 1 kHz, 2 kHz, 4 kHz, 8 kHz or 16 kHz and relative bandwidth 20% were used. The velocity spectra are plotted in Fig 6 (the amplitudes of the plots corresponding to the two TMAPs have been normalized) and show good responses at the matched velocities. It can be shown that it is possible to obtain satisfactory responses for BPFs with centre frequencies up to the Nyquist frequency (50 kHz in this case). The responses to SFAPs generated from both the TMAPs are identical in the sense that the values of Q_v measured at the matched velocities are the same in both cases. These results support the assertion that the bandpass filtered velocity selectivity depends only on N, f_0 and v and some physical constants, *not* on the characteristics of the TMAP function, as is the case for IVS. The values of Q_v are listed in Table 1 together with values calculated from eqn (4). The calculated values fit the simulated ones very well.

3.2. Simulated results with additive noise

Zero-mean white Gaussian noise was added to the system in a manner consistent with the approach adopted in [1] (i.e., 11 sources of uncorrelated voltage noise were introduced, one at the input to each *monopolar* channel). These noise sources represent the total noise present in each channel referred to the

input. As noted in [1] the total input-referred noise is the sum of several individual sources that are assumed to be independent and uncorrelated. The *signal-to-noise ratio* (SNR) was defined as the ratio of the *r.m.s.* value of signal (i.e. TMAP) to noise over a sequence of standard length (10.23 ms, corresponding to 1024 samples), referred to the input.

In order to test the effect of the noise on the system and in particular on the ability of the BPFs to increase the velocity selectivity compared to IVS, the simulations described in Section *A.* were repeated with varying levels of additive white Gaussian noise. The results are presented in Table 2 for three values of SNR (1, 10, 100) for each of the two TMAPs. The frequency in column *A* for each value of SNR gives the maximum frequency (f_{omax}) at which an intelligible output is obtainable from a BPF centred at that frequency. Once f_{omax} has been determined, the maximum available velocity selectivity (Q_v) can be calculated from eqn (10) (column *B*) and the enhancement factor found (i.e. compared to IVS-column *C*). In general TMAP#2 performs better than TMAP#1, due to the wider bandwidth of the signal. There is thus more energy at higher frequencies in SFAPs generated from TMAP#2, whilst the additive noise has the same spectral density at all frequencies and for both TMAPs. In the worst case considered, with SNR set to unity, there is no enhancement in Q_v for TMAP#1, whilst for TMAP#2 a modest enhancement of about 3.5 is possible. For SNR = 10 the values increase to 2 and 7 respectively and 4 and 7 respectively for SNR = 100, although in this case, higher values could be obtained for TMAP#2 if more bandwidth were available.

4. Discussion

4.1 Limitations of the theory

The use of bandpass filters to improve the selectivity of VSR systems was first proposed in [9, 1] and the current paper extends and develops these methods. After briefly summarising the basic theory of the method, the effects of key filter parameters, in particular centre frequency and filter order are examined. The proposed system uses digital bandpass filters and for the purposes of this paper these were implemented in software, using MATLAB. Since it is likely that a real VSR system would use similar BPFs, whether implemented in software or hardware, the results of the simulations presented in this paper can be considered to be quite reliable and representative.

4.2 Limits of available selectivity with and without noise

In Section 2.4 it was suggested that the factors limiting available velocity selectivity are (i) the spectral bandwidth of the TMAP function, (ii) the analogue bandwidth of the signal capture/acquisition system,

(iii) the resolution of the digitisation process (ADC) and, (iv), noise. Furthermore, if digitisation with 10-bits resolution is assumed, in the absence of noise, the level of available velocity selectivity is limited by (i) and (ii). It was then demonstrated that in the case of TMAP #1, ADC resolution set the limit whilst for TMAP #2, with its wider spectrum, analogue bandwidth (which in turn is limited by the sampling rate/Nyquist frequency) was the limiting factor. However, these considerations are purely hypothetical and the introduction of *noise* tends to alter the situation completely. Uncorrelated white Gaussian noise was added to each monopolar input as suggested in [1]. Since the input-referred noise spectrum is flat in contrast to those of the TMAPs, the presence of noise has most influence at higher frequencies where the signal spectral density is lowest. The resulting bandwidth restriction in turn limits the available velocity selectivity, both IVS and FVS. So, although the effect of bandpass filtering removes the influence of the TMAP spectrum on the value of Q_v at a particular frequency, the maximum available value of Q_v *will* depend on the TMAP function, because of the effects of noise. In spite of the restrictions imposed by noise, very useful enhancements in selectivity are nonetheless predicted for both TMAPs, especially TMAP #2, as detailed in Table 2.

4.3 The effect of image responses

The formation of spurious responses ('images') was discussed in Section 2.6. For the example shown in Fig 6, d = 3mm, τ = 100 μs (i.e. for v_o = 30 m/s) and so for the 16 kHz BPF, velocity spectral images would be expected at 13.3 m/s, 18.5 m/s and 80 m/s. The lower velocity images are clearly visible in both figures, the higher velocity signal being outside the range shown. As already noted, the amplitude and range of occurrence of these images depend on N and W, while W depends on the BPF parameters, especially the filter order and relative bandwidth and can often be quite small in comparison with genuine outputs from excited populations. Note that there is no possibility of confusing a genuine output with an image since the former will occur at the *same velocity* in the spectra calculated at all filter outputs whilst images will appear at velocities dependent on f_o.

In conclusion, this paper presents a practical method to improve the performance of VSR systems compared to currently available methods. The use of BPFs provides a significant increase in velocity selectivity which will form the basis of new systems to widen the application of the method beyond the current state-of-the-art which is restricted to the recording and analysis of CAPs.

References

1 Donaldson N, Rieger R, Schuettler M & Taylor J (2008) Noise and Selectivity of Velocity-Selective Multi-Electrode Nerve Cuffs. Med. & Biol. Eng. & Comput., 46 (10), 1005-1018.

2 Haugland, M et al (1997) Restoration of lateral hand grasp using natural sensors. Artificial Organs 21 (3): 250-253.

3 Hoffer J, Loeb G, Pratt C (1981) Single Unit Conduction Velocities from Averaged Nerve Cuff Electrode Records in Freely Moving Cats. Journal of Neuroscience Methods, 4:211-225.

4 Hoffer, J (1990) Techniques to study spinal cord, peripheral nerve and muscle activity in freely moving animals. In: Neuromethods, 15: Neurophysiological Techniques: Applications to Neural Systems. 65-145, Boulton, A.A., Baker, G.B., Vanderwolf, C.H. (eds), The Humana Press Inc., Clifton, NJ.

5 Rieger R, Schuettler M, Pal D, Clarke C, Langlois P, Taylor J & Donaldson N (2006) Very low-noise ENG amplifier system using CMOS technology. IEEE Trans Neural Syst Rehabil Eng. 14(4): 427-37.

6 Rieger R, Taylor J, Comi E, Donaldson N, Russold M, Jarvis J, Mahoney C, & Mclaughlin J (2004) Experimental Determination of Compound A-P Direction and Propagation Velocity from Multi-Electrode Nerve Cuffs. Medical Engineering & Physics, 26: 531-534.

7 Rosenfalck, P (1969) Intra- and extracellular potential fields of active nerve and muscle fibers - A physico-mathematical analysis of different models. Ph.D. thesis, Akademisk Forlag, Copenhagen University.

8 Struijk J (1997) The extracellular potential of a myelinated nerve fibre in an unbounded medium and in nerve cuff models. Biophys. J., 72:2457-2469.

9 Taylor J, Donaldson N, & Winter J (2004) The use of multiple-electrode nerve cuffs for low velocity and velocity-selective neural recording. Med. & Biol. Eng. & Comput., 42 (5), 634-43.

10 Van Veen, B et al (1992) Potential distribution and single-fibre action potentials in a radially bounded muscle model", Med. & Biol. Eng. & Comput, 30 (5): 303-310.

11 Yoshida K, Kurstjens G, & Hennings K (2009) Experimental validation of the nerve conduction velocity selective recording technique using a multi-contact cuff electrode. Medical Engineering & Physics 31: 1261-1270.

List of Figure Captions

Figure 1. This shows a *multielectrode cuff* (MEC) connected to a *tripolar* (double differential) amplifier array. The *N* tripolar outputs (where *N* is typically about 10) are digitised and processed in the signal processing unit on the right of the figure. For an action potential (AP) propagating symbolically downwards, voltages are induced sequentially at the electrodes which result in the appearance of tripolar output signals. The delay between the appearances of successive outputs depends on the propagation velocity of the AP and the inter-electrode spacing of the MEC and allows a simple calculation of the AP velocity. The calculation process is carried out in the digital domain using the programmable delays indicated. Finally, the bandpass filter (BPF) is used to improve the velocity selectivity as described in the text. We refer to the velocity spectrum calculated at the output of the adder as the *intrinsic velocity spectrum* (IVS) and that at the output of the BPF, the *filtered velocity spectrum* (FVS).

Figure 2. Time and intrinsic velocity domain responses of the system shown in Fig 1 (output of the adder), with a propagation velocity of 30 m/s. Subplot (a) shows the time domain response of the system, each curve corresponding to a different *matched velocity*, the SFAP being generated from TMAP#1. The three peaks of the waveforms are labelled α, β & γ. Subplot (b) shows the intrinsic velocity spectrum (IVS) for TMAP#1 derived from Fig 2(a) measured at points α (top curve) and β (bottom curve). Subplot (c) shows the same calculation using TMAP #2. The parameters of the TMAP function ($x(t) = At^n e^{-Bt}$) are included.

Figure 3. Plot (a) shows the time record of the output of an 8^{th} order Butterworth bandpass filter of 20% relative bandwidth stimulated with a narrow pulse of unit amplitude. Plot (b) shows three sinusoids, each representing the central half-cycle of the output of a channel BPF. The amplitudes have been normalised to unity and the delay offset τ is the naturally-occurring inter-channel delay. *N* sinusoids are summed to calculate the velocity selectivity of the system.

Figure 4. Frequency domain spectrum (FFT) of a 9-tripole system driven by SFAPs generated by TMAPs #1 and #2. The propagation velocity is 30 m/s and the system is matched at that velocity. Note that the spectral amplitude generated by TMAP #1 declines with frequency much more rapidly than that generated by TMAP #2. The sampling rate is 100 ks/s.

Figure 5. Time domain responses (insets) and corresponding bandpass filtered spectra at the output of a VSR system (derived from TMAP #1 and matched at 30 m/s-see Fig 4) compared to the unfiltered (IVS) spectrum. The unfiltered output is passed through Butterworth BPFs with centre frequency (f_o) 8 kHz and order (p) 2, 4 and 8 and with 20% relative bandwidth. For the $p = 2$ filter the spectral amplitude at frequencies in the 'baseband' range 0-5 kHz is larger than at f_o, suggesting significant breakthrough in the passband and the need for a BPF with $p = 4$, at least.

Figure 6. Bandpass filtered version of the time domain IVS plot shown in Fig 2 and comparing the differences between SFAPs generated using TMAP functions #1 (dashed line) and #2 (dotted line) with a propagation velocity of 30 m/s. The filters are 8^{th} order Butterworth digital units with centre frequencies f_0 are (a) 1 kHz, (b) 2 kHz, (c) 4 kHz, (d) 8 kHz, (e) 16 kHz and (f) 32 kHz. There is no significant difference between the two responses and the corresponding values of Q_v are 1.4, 2.9, 5.7. The velocity step is 1 m/s and there is no additive noise. Note the formation of spurious 'image'

responses at velocities in the region 10-30 m/s as discussed in section 2.6 (those occurring at higher velocities occur ‘out of band’). For the 16 kHz BPF these occur at 13.3 m/s, 18.5 m/s and 80 m/s (out of range) as discussed in the text. The spectral velocities of the images are dependent on the BPF centre frequency and so are easily distinguished from the response to an excited population which does not. Note that the peak amplitudes of the two plots have been normalized.

List of Acronyms Used in the Text

BPF	Bandpass filter
FFT	Fast Fourier transform
ADC	Analogue to digital converter
SNR	Signal to noise ratio
VSR	Velocity selective recording
SFAP	Single fibre action potential
TMAP	Transmembrane action potential
CAP	Compound action potential
MEC	Multi-electrode cuff
IVS	Intrinsic velocity selectivity
BPFVS	Bandpass filtered velocity selectivity

Table 1

Comparison of Simulated and Calculated Values of Q_v for a 9-Channel Filtered VSR System for a Single SFAP with propagation Velocity 30 m/s

BPF Centre Frequency, f_0 (kHz)	TMAP #1	TMAP #2	Calculated value*
1	0.8	0.8	0.8
2	1.9	1.9	2.0
4	4.3	4.0	4.2
8	7.5	7.5	8.5
16	17.0	16.0	17.1
32	33.3	33.3	34.2

*Calculated using equation (4)

Table 2

Simulated maximum available velocity selectivity (Q_{vmax}) as a function of signal-to-noise ratio for a 9-tripole system. The input is an SFAP propagating at 30 m/s and the limiting resolution is 10-bits

SNR	**1**			**10**			**100**		
	f_{omax} (kHz)	Q_{vmax}	$\frac{Q_{v\max}}{Q_{vivs}}$	f_{omax} (kHz)	Q_{vmax}	$\frac{Q_{v\max}}{Q_{vivs}}$	f_{omax} (kHz)	$Q_{v\,max}$	$\frac{Q_{v\max}}{Q_{vivs}}$
TMAP#1	4	2.9	1	8	5.7	2	16	12.5	4
TMAP#2	16	12.5	3.5	32	25	7	32	25	7*

f_{omax} is the maximum available frequency which gives the maximum velocity selectivity Q_{vmax}; $\frac{Q_{v\max}}{Q_{vivs}}$ compares this maximum with the IVS.

*limited by analogue bandwidth (32 kHz)

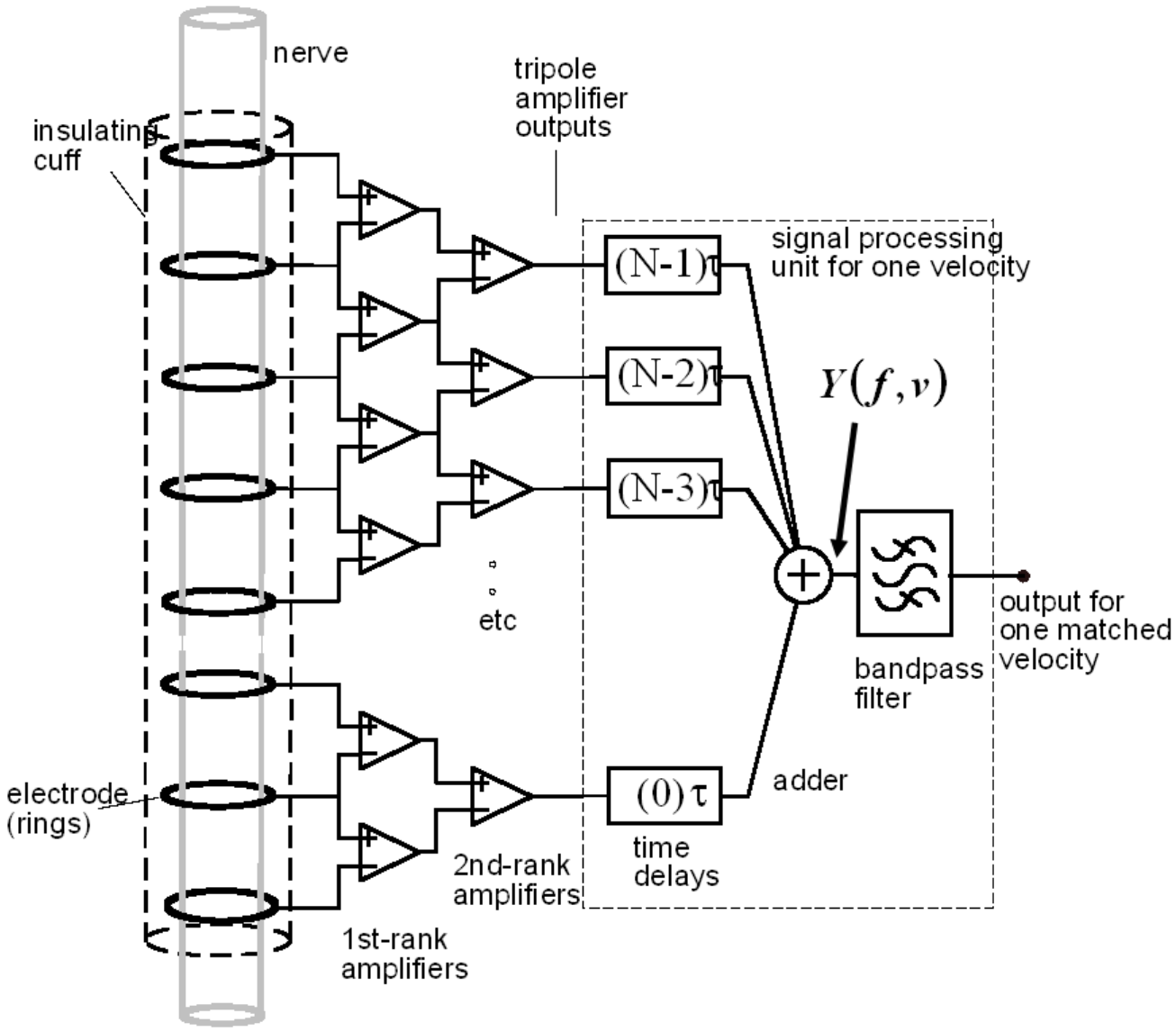
nerve
tripole amplifier outputs
insulating cuff
signal processing unit for one velocity
(N-1)τ
(N-2)τ
(N-3)τ
$Y(f,v)$
etc
output for one matched velocity
bandpass filter
adder
(0)τ
time delays
electrode (rings)
2nd-rank amplifiers
1st-rank amplifiers

Figure 1

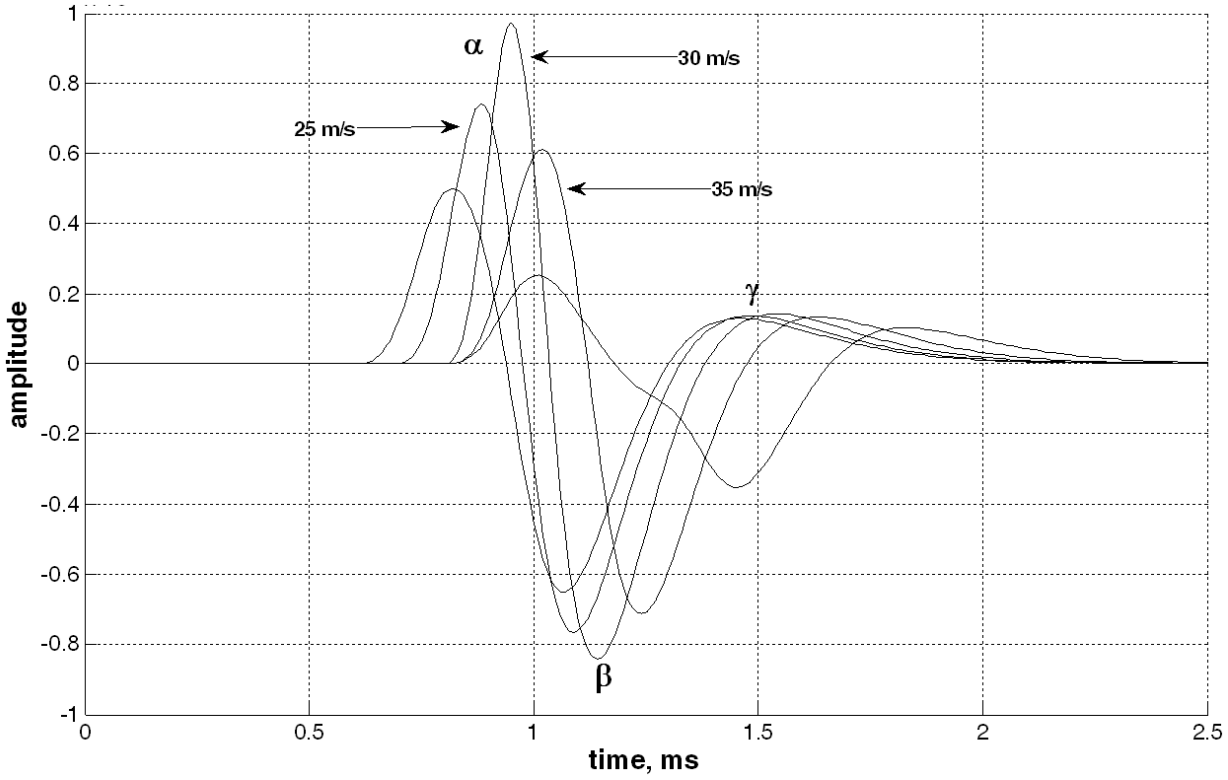
α
30 m/s
25 m/s
35 m/s
γ
β
amplitude
time, ms

(a)

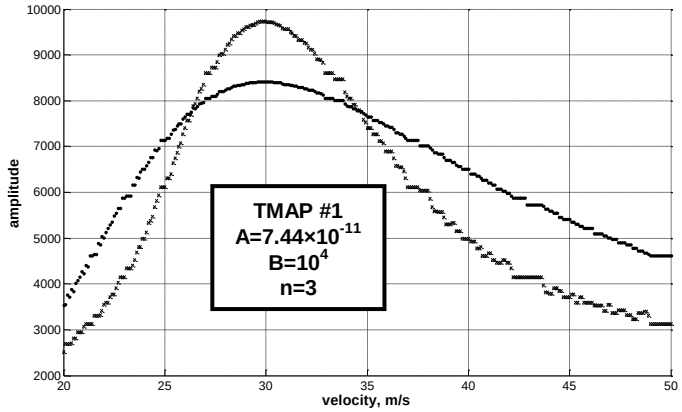
TMAP #1
A=7.44×10^-11
B=10^4
n=3
amplitude
velocity, m/s

(b)

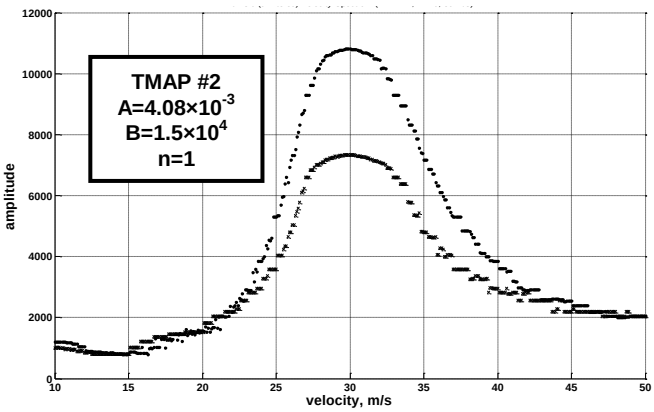
TMAP #2
A=4.08×10^-3
B=1.5×10^4
n=1
amplitude
velocity, m/s

(c)

Figure 2

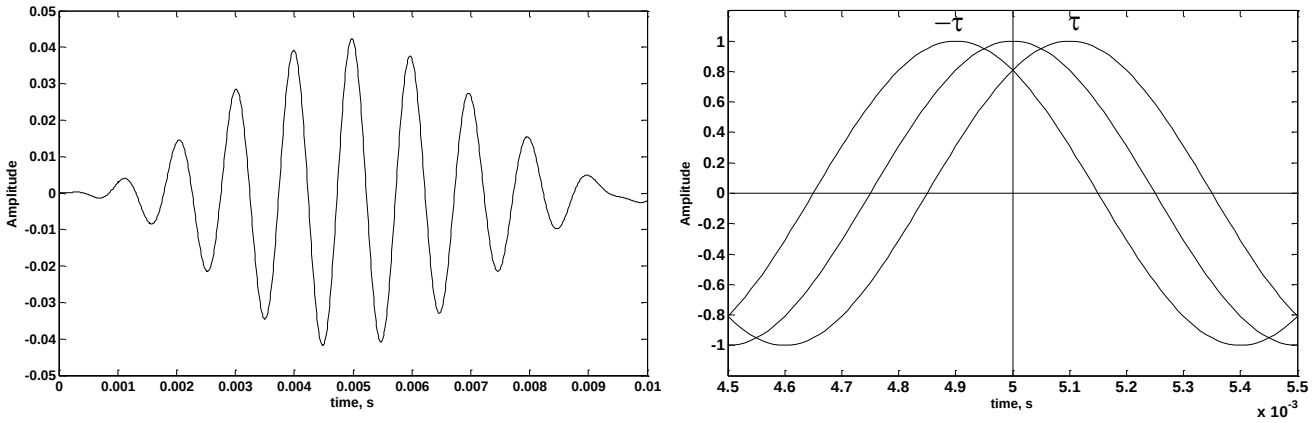

(a) (b)

Figure 3

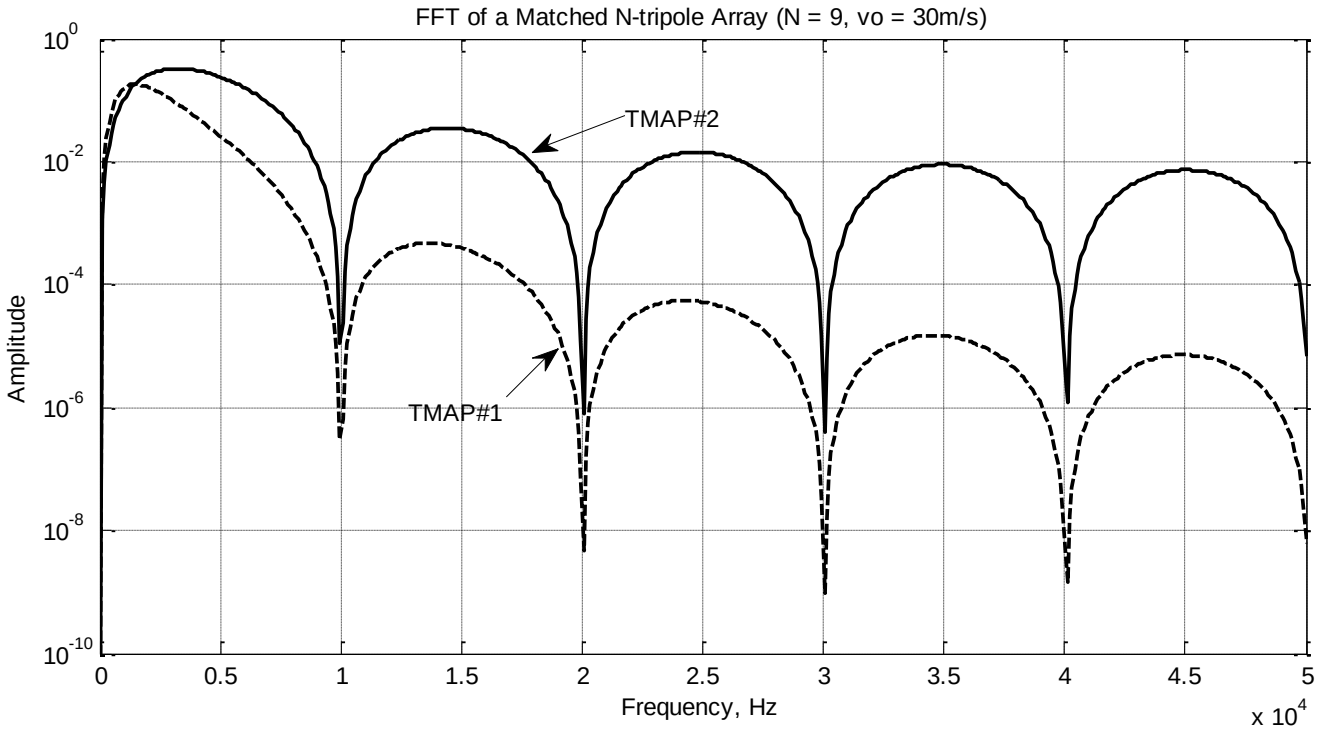

Figure 4

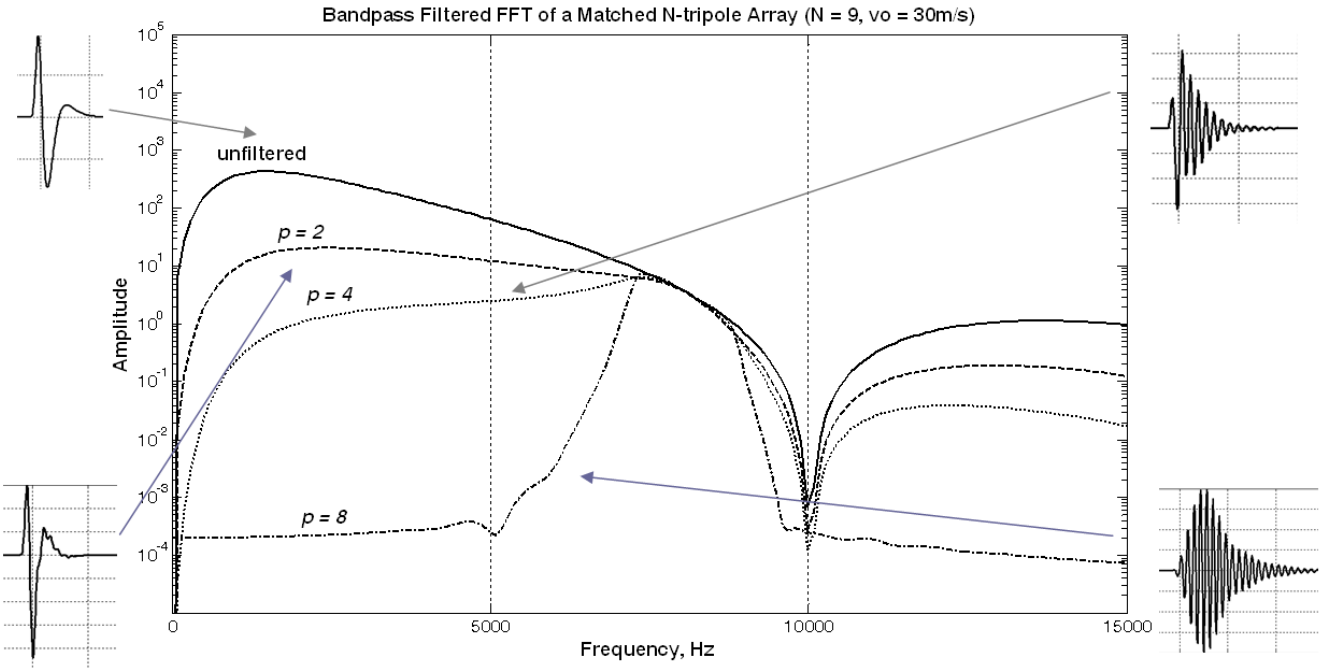
Bandpass Filtered FFT of a Matched N-tripole Array (N = 9, vo = 30m/s)
unfiltered
p = 2
p = 4
p = 8
Amplitude
Frequency, Hz
0
5000
10000
15000

Figure 5

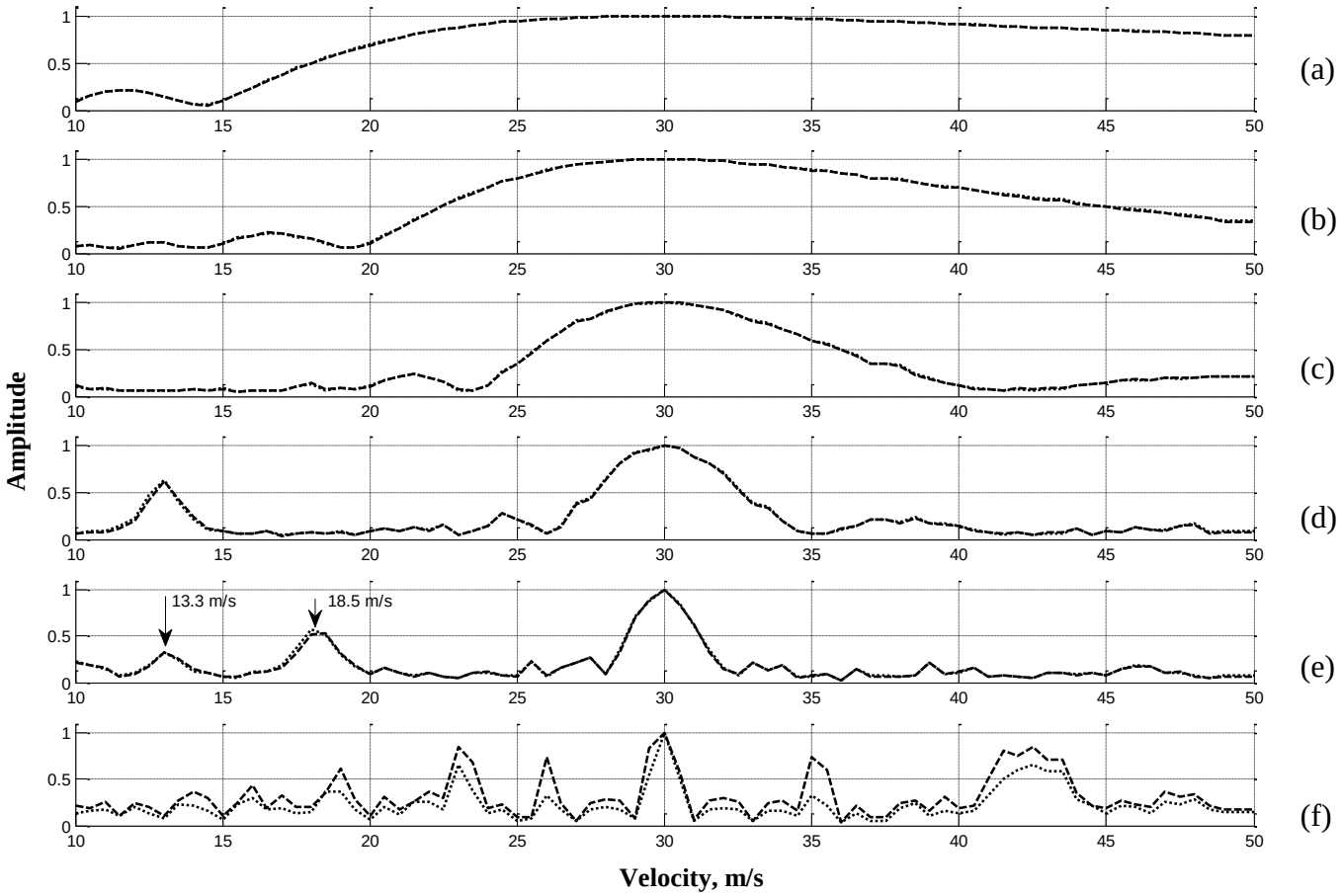

Figure 6